An optical scanning system for spectroscopic impurity flux investigations inside the ASDEX tokamak

G. Fussmann, J. V. Hofmann, G Janeschitz, J. Szigeti*

* Central Research Institute for Physics, Budapest, Hungary

IPP III/152 October 1989

MAX-PLANCK-INSTITUT FÜR PLASMAPHYSIK

8046 GARCHING BEI MÜNCHEN

MAX-PLANCK-INSTITUT FÜR PLASMAPHYSIK

GARCHING BEI MÜNCHEN

An optical scanning system for spectroscopic impurity flux investigations inside the ASDEX tokamak

G. Fussmann, J. V. Hofmann, G Janeschitz, J. Szigeti*

* Central Research Institute for Physics, Budapest, Hungary

IPP III/152 October 1989

Die nachstehende Arbeit wurde im Rahmen des Vertrages zwischen dem Max-Planck-Institut für Plasmaphysik und der Europäischen Atomgemeinschaft über die Zusammenarbeit auf dem Gebiete der Plasmaphysik durchgeführt.

Abstract

A scanning mirror system was developed to resolve impurity flux sources spatially across about 2/3 of the ASDEX surface by using visible spectroscopy. A totally computer-controlled layout allows wide-range spatial scanning during a discharge. Spectra over a range of ~150 Å are recorded with an integration time down to 20 ms. The versatility of this new system is illustrated by means of first observations of ASDEX discharges with additional heating (NI, LH, ICRH) and modulated gas puffing experiments.

CONTENTS:

I. Introduction

Plasma spectroscopy in its application to tokamaks and stellarators has hitherto been mainly concentrated on the short-wavelength range in the VUV and soft X-rays. This limitation was governed by the fact that high-temperature plasmas ($T_e \geq 100$ eV) produce line radiation almost exclusively in this spectral range. During the last few years, however, visible spectroscopy has gained increasing attention for a number of reasons. First of all, there are technical advantages such as the possibility of using lenses and fibers, and the little effort needed to achieve high spectral resolution. On the other hand, there are several important physical questions that can be addressed in the visible or near UV range: apart from the investigation of forbidden transitions (magnetic dipole radiation), particular interest has been shown in beam-induced CX recombination of impurity ions and line emission from the plasma edge region. Charge exchange recombination spectroscopy (CXRS) is meanwhile widely used to measure ion temperature profiles and concentrations of low-Z impurities such as He, C and O [1]. He^+ edge radiation has recently been investigated to determine radial electric fields by poloidal and toroidal rotation measurements [2]. In the majority of cases, however, edge radiation from neutral or singly ionised atoms has been measured to determine local influxes of impurities [3-6]. For technical reasons these measurements are generally restricted to observation of preselected surfaces such as limiters, divertor plates or antennae where pronounced plasma-wall interaction is expected.

In view of the great importance of impurities for the whole fusion program it is highly desirable to obtain as much information as possible about the local origin and temporal dependence of the various impurity influxes. The question of the spatial distribution of the influxes is emphasised for a divertor tokamak like ASDEX since here the dominant role of a limiter with respect to erosion and recycling is lacking.

For this purpose we have designed and constructed a special mirror scanning system which allows us to observe about 2/3 of the total surface of the main plasma chamber. The system is equipped with a visible spectrometer of sufficient resolution to distinguish clearly between the numerous lines from metals (Fe, Cr, Cu) and light impurities (He, C, N, O). Spatial scanning can be performed either on a shot-to-shot basis or within a single discharge. A diode array camera mounted at the exit plane of the spectrometer allows us to take up to 200 spectra per discharge and to trace the temporal behaviour of several impurity lines simultaneously. In addition to 3D-plots of the time-dependent spectra, a qualitative assessment of plasma-wall interaction can be made from video pictures taken along the same path of light.

In the following, we give a detailed description of the system and present some first illustrative measurements. First results during ICRH heating were recently published in [7].

II. The mechanical arrangement

A block diagram of our experimental setup is shown in Fig. 1. The plasma light coming from a point P inside the tokamak is projected via a mirror (m_1) through two quartz lenses (L_1, L_2) onto the entrance slit of a grating spectrometer (Czerny-Turner mount, 1200 grooves/mm, f = 1 m). The rotatable mirror head itself consists of a water-cooled copper finger on both sides of which quartz plates are mounted. The quartz plates, 120 mm x 60 mm x 3 mm each, are coated with aluminum and coverd by a SiO_2 protection layer. The side-ends of the copper finger and the mirrors are covered with protective carbon tiles. The mechanical arrangement (see Fig. 2.), which holds the mirror, can radially be shifted in a flexible bellows tube along the major radius of the torus (indicated by *L*). The mirror is able to rotate around this radial axis (*R*) and in addition around an axis perpendicular to it (*S*). The movement with respect to all three degrees of freedom is provided through three step-motors (M_1-M_3) which are controlled, by means of three absolute encoders (E_1-E_3) and a RS-232 interface, via a CAMAC interface by our UNIX computer system (see Fig. 1). The computer-controlled step-motor system also provides the possibility of scanning along a partial area of the tokamak one or several times during a discharge. While scanning on a shot-by-shot basis is routinely performed, scans during a discharge have hitherto been restricted to within the poloidal or toroidal plane. In this case the mirror only rotates around one axis at a time.

By using the possibility of scanning during a plasma shot, the scanning velocity can be preset from 0 to about 3,000 steps per second, resulting in 4.5 full poloidal scans (full turns of the mirror) during a shot of about 3 s duration. The readout of spectra during such a scan can be taken at frequencies of up to 50 Hz. This results in 33 subdivisions of a scan and a corresponding number of spectral readouts. For each readout the position of the mirror at the readout time is supplied. The constant scanning velocity and the readout frequency determine the range and number of iterations of a scan during a discharge and are only limited by the 20 ms minimum integration time of the Reticon camera. Two-dimensional scans are also possible but, since the scanning velocity can not be changed during a shot, it is not possible, for example, to scan toroidally along the divertor entrance slit. This would require programmed variation of the scan velocities around two axes of the mirror, which is not yet available.

The accessible area inside the ASDEX tokamak, covering about 2/3 of the whole inner surface of the main plasma chamber, including one of the ICRH antennae, is shown in Figs. 3 a and b. In particular direct observation of the divertor entrances, the SE neutral beam, the ICRH-SE antenna, the SE gas valve, the pellet centrifuge and the laser ablation is of great importance (see Figs. 5, 7-10).

III. The optical setup

The schematic arrangement of the optical system is shown in Fig. 4 a. The first lens (L_1) inside the bellows tube (f = 200 mm, Ø = 70 mm) provides image reduction between 6:1 and 12:1, depending on the distance of the point P investigated in the torus. The image plane of the farthest accessible point inside the tokamak (≈4 m from the mirror) is 21.4 cm behind this lens, whereas for the nearest point (≈1.5 m) it is 23 cm. The position of the second lens (L_2) outside the vacuum system (f = 500 mm, Ø = 60 mm) is 206 cm from the first one and 69 cm from the spectrometer. It projects the image onto the entrance slit of the grating spectrometer with a second image reduction of 3:1. The resulting transformation from a point P inside the tokamak onto the entrance slit of the spectrometer is therefore between 18:1 and 30:1. The quartz window of the vacuum system (Ø = 70 mm) between the two lenses is at a distance of 66 cm from L_1. The aperture of the complete system is determined by the diameter of the outer lens L_2 and its distance from the entrance slit of the spectrometer and is about 1:15. The geometrical resolution of the system inside the tokamak, perpendicular to the entrance slit of the spectrometer (usually 100 µm wide), is 2 mm at the optimal distance, and even in the two limiting positions it is better than 5 mm.

The actual optical arrangement is depicted in Fig. 4 b. Between the window (W) and the second lens (L_2), a plane parallel quartz plate beam-splitter (q) is mounted at 45^o, which allows simultaneous viewing with a CCD video camera.

Using a video tape recorder (V.T.R.) and a video hardcopy (V.H.C), we can record and plot the pictures of the CCD camera. The video recorder provides a temporal resolution of about 20 pictures per second. The use of special filters in front of the video camera makes it easier to distinguish between the various impurities. Because of the relatively large visible area of the video camera it is possible to discern patterns and changes of the light sources. Some interesting parts of the tokamak, viz. the graphite covered plates forming the divertor entrance and the bottom of the ICRH antenna, recorded by the CCD camera, are shown in Figs. 5 a-c.

At the exit plane of the spectrometer we use an intensified Reticon diode-array camera with 1024 pixels (25 μ x 2.5 mm each). Because of cross-coupling problems the minimal spatial resolution is about 3 pixels. In conjunction with a reciprocal dispersion of 8 Å/mm (first order) of the spectrometer, we thus achieve a spectral resolution of $\Delta\lambda \approx 0.6$ Å or $\lambda/\Delta\lambda \approx 10^4$. The integration time of the camera can be arbitrarily chosen between 20 μs/pixel and several seconds, yielding a whole spectrum every 20 ms.

Setting the spectrometer to a selected wavelength, maintains a spectrum of about ±75 Å on the diode-array camera. The whole accessible spectral range of the camera from 2500 Å to 8000 Å is covered by about 40 different wavelength settings.

Since the whole mirror system has not yet been absolutely calibrated, no absolute values for the impurity influxes have been determined. In spite of this we obtained some interesting results, which are presented in section VI.

To allow comparison of spectra under different plasma conditions and from different observation points, we have so far had to restrict our investigations to just a few spectral ranges. In several special cases we used the higher order of refraction of the spectrometer to get better dispersion, although the intensities became significantly smaller. Nevertheless the B IV lines, for example, at 2821.7 - 2825.9 Å could easily be measured in 4th order.

IV. Data acquisition and processing

Initialisation and wavelength and mirror settings or other parameter changes are all computer-controlled by means of a diagnostic program running on a Unix workstation. All spectra (usually 200) recorded during a discharge together with the shot number and the whole parameter set of the measurement are stored in a general external memory, from where they are accessible at any time later on.

Between successive shots (≈10 - 15 min) the recorded data are processed and printed out by a laser writer as two-dimensional spectra at selected time points, as three-dimensional spectra for the whole discharge and as time evaluations of selected line intensities (see Figs. 7 - 10). The different impurity lines occurring in the spectra are automatically identified by the plot program using identification tables (see Tab. 1) and indicated in the plots. Because of the multitasking capabilities of the computer system data acquisition and storage as well as processing and plotting are done simultaneously. Owing to the fast output of a laser writer all necessary information from the last shot is available to change the parameters for the next shot.

V. Coordinate transformations

The position of a selected point P inside the tokamak is usually given in toroidal coordinates (r, Θ, Φ); see Fig. 6. In our case the radius r is measured from the plasma center in the horizontal midplane of the tokamak, indicated by the dashed line and the major radius R_0 (= 1.65 m). The poloidal angle Θ is measured out of the midplane in contrast to the usual convention of measuring it from the vertical z-axis. The toroidal angle Φ in the midplane is chosen to be zero at the toroidal position of our mirror system.

On the other hand, the exact position and orientation of the scanning mirror is provided by the step numbers (L, R, S) of its encoders (see also Fig. 2). These step numbers are associated to the following movements of the mirror:

- L: the longitudinal position of the mirror from the torus center, denoted by L_t $L_t = R_o + l_o$ - Lm, (Lm = L/200200, Lm in meters, L in steps, l_o = 1.44 m, Lm = 0 at the virtual mirror origin O´, where L = 0);
- R: the rotation of the mirror around the radial axis (O´- m1) by the angle α out of the torus midplane.
- S: the movement of the mirror´s surface vector within the plane (O´- m1- P) by the angle β.

The angles α and β defined in this way actually represent the rotations of the mirror. The distance of the selected point P from the mirror is denoted by ρ. The transformation between the toroidal coordinates (r, Θ, Φ) and the step numbers (L, R, S) is not unique since the longitudinal position L of the mirror may be chosen arbitrarily. For a selected value of L, however, the transformation from (r, Θ, Φ) to $(\rho, R, S)_L$ is unique and the step numbers R and S associated with the selected point P can be calculated as described in the appendix.

VI. First experiments

As a "standard spectral range" we chose the region around λ = 4300 Å. As seen in Fig. 7 a, the spectrum in this range is dominated by lines of carbon (C II, λ = 4267.0 Å, 3d ^{2}D - 4f ^{2}F^o), deuterium and hydrogen (D_γ, λ = 4339.3 Å; H_γ , λ = 4340.5 Å, 2p ^{2}P^o - 5d ^{2}D) and two sets of oxygen (O II, λ = 4317.1 Å, 4319.9 Å, 4325.8 Å, 4336.9 Å , 4345.6 Å, 4349.4 Å, 4366.9 Å, 3s ^{4}P - 3p ^{4}P^o and 4347.4 Å, 4351.3 Å, 3s´ ^{2}D - 3p´ ^{2}D^o). In the case shown the spectrum is taken in the horizontal midplane of the tokamak viewing towards the ICRH-SE antenna; see Figs. 3 a, b. Additional heating was supplied from 1.4 - 1.8 s (neutral injection, P_{NI} = 2 MW) and 2.1 - 2.5 s (lower hybrid, P_{LH} = 1.4 MW). In addition to the above-mentioned lines, a multiplet of three chromium resonance lines (Cr I, λ = 4254.4 Å, 4274.8 Å, 4289.7 Å, $3d^5\,4s^1\,{}^7S_3$ - $4p^1\,{}^7P_{4,3,2}{}^o$) emerges during lower hybrid operation. The large increase of the line emission with the onset of NI and, even

more, LH heating is quite drastic. The CH molecular bandhead near λ = 4310 Å is also visible but not very pronounced. (The parameters of this shot #28350 are: B_t = 2.8 T, I_p = 275 kA, $\langle n_e \rangle = 3.6 \times 10^{13}$ cm^{-3}, slit 100 µm x 6 mm, readout 50 Hz.)

This "standard spectral range", containing lines of the most abundant light impurities in ASDEX, oxygen and carbon, as well as the strong chromium lines (produced by sputtering from stainless-steel surfaces), allows the machine conditions and the impurity production level to be monitored.

Comparison of the NI- and LH-heated phases in Fig. 7 b reveals a much higher increase of the intensities during the LH phase, despite the smaller power supplied (P_{NI} = 2 MW, P_{LH} = 1.4 MW). The increase in the intensity from NI to LH is about equal for the C II and Dγ signals ($I_{C\ II}$ (LH)/$I_{C\ II}$(NI) = 3.5, $I_{D\gamma}$(LH)/$I_{D\gamma}$(NI) = 3.7), while the increase in the Cr I and O II signals is larger (I_{CrI}(LH)/I_{CrI}(NI) = 4.4, I_{OII}(LH)/I_{OII}(NI) = 4.8). This indicates enhanced erosion of chromium and detachment of oxygen in the case of LH operation.

As a second example we show in Fig. 8 a spectrum around λ = 3250 Å. The spectrum is again taken looking onto the ICRH antenna. The intensities are rather small during the initial ohmic phase. Two copper resonance lines (Cu I, λ = 3247.5 Å and 3274.0 Å, 4s $^2S_{1/2}$ - 4p $^2P_{1/2,\ 3/2}$) are marginally to be seen around 0.1 s and later at 1.0 s, when neutral injection was switched on (P_{NI} = 1.6 MW). With the onset of ICRH heating at 1.1 s (P_{ICRH} = 1.5 MW) a whole set of titanium lines (Ti I, II) appears and drops off when the ICRH is switched off at 1.9 s. The high titanium fluxes are due to sputtering of Ti out of the TiC layer covering the antenna faraday screen as soon as the antenna is activated. During ICRH operation Ti lines can be seen throughout the lower part of the whole visible spectrum from 3000 Å to 5000 Å when looking at the antenna, but can hardly be detected elsewhere. Despite the high Ti fluxes observed at the antenna, the overall influx of Ti into the plasma is relatively small owing to the small antenna surface in relation to the whole surface of the tokamak. (The shot parameters are: #28287, B_t = 2.3 T, I_p = 420 kA, $\langle n_e \rangle = 5.7 \times 10^{13}$ cm^{-3}, slit 100 µm x 6mm, readout 50 Hz.)

As an example of a poloidal scan during a discharge (see Fig. 3 b) we show a spectrum around λ = 6540 Å, Fig. 9 a. This spectral range contains the two resonance lines of copper, already mentioned above, in second order (Cu I, 2nd order, λ = 3247.5 Å, 3274.0 Å), the Balmer α-lines of deuterium and hydrogen (D_α, λ = 6561.0 Å; H_α, λ = 6562.8 Å, 2p $^2P^o$ - 3d ^2D) and two carbon lines (C II, λ = 6578.0 Å, 6582.9 Å, 3s ^2S - 3p $^2P^o$). In addition, the neutral beam components during neutral injection heating from 1.6 - 2.5 s (P_{NI} = 1.6 MW) occur when the viewing line intersects the neutral beams during the scan. Furthermore, the C II lines as well as the D_α, H_α lines show Zeeman splitting in the

magnetic field. The Cu I signals, only to be seen in one of the successive spectra respectively, mark the inner divertor slit and result from the water-cooled Cu shields in both divertors. Since the mirror scans a poloidal cross-section of the ASDEX vessel several times during the discharge, the time axis in Figs. 9 a, b is actually a space coordinate. The very sharp Cu I signals are to be distinguished from the D_α/H_α and C II signals (broader spatial distribution), which show synchronized temporal behaviour and a similiar intensity structure, Fig. 9 b. The scan clearly indicates that the only visible copper source is the divertor throat. Deposited copper, however, can be eroded from the ICRH antenna during ICRH heating, Fig. 8.

The D_α/H_α signals can be resolved in second order to yield the D/H mixture in the plasma, a quantity of particular importance for ion temperature measurements from neutron rates, isotope effect studies and ICRH minority heating. From the Zeeman splitting of the C II lines the local magnetic field in the edge region can be determined. The Zeeman splitting of the C II lines is best observed in the particular case when we look in the direction parallel to the magnetic field (toroidal field of the tokamak, view tangential to inner wall). In this particular case two well-separated, circularly polarized σ-components result, while the central π-component is surpressed, as observed in toroidal scans. The components of the neutral beams reveal the species mix of the beams, while the Stark splitting of these components (not resolved in Fig. 9 a) may possibly be used to determine the local poloidal magnetic field [8].

Finally, a case of modulated H_2S-gas puffing during the discharge is shown in Fig. 10 a. Here the mirror looks direct onto the gas valve (see Fig. 7 a) slightly below the midplane. A residual signal of the sulphur multiplet (S II, λ = 5428.6 Å, 5432.8 Å, 5453.8 Å, 5473.6 Å and 5509.7 Å, $3p^24s^4P - 3p^2(3P)4p^4D^o$), which can be seen even before the puffing starts, results from sulphur left in the tokamak from the previous shot. The sinusoidal 5 Hz modulation of the gas valve is reflected in the temporal behaviour of the spectra, Fig. 10 b. The phase shift of the spectra, compared to that of higher ionisation stages measured farther inside the plasma in the VUV and X-ray range, allows one to study transport phenomena and deduce diffusion coefficients.

VII. Conclusions

The variety of these experiments has demonstrated the advantages of the scanning system described. Selected surfaces and structures in ASDEX can be investigated to determine impurity influxes and yield a variety of additional information. The system has been routinely used to time-trace and monitor the machine conditions during additional heating and after boronisation and carbonisation of the ASDEX vessel.

For future experiments we are planning to position additional fixed mirrors inside the tokamak to allow measurements of poloidal rotation. Furthermore, absolute calibration of the whole system will be provided for the next experimental period. In addition to impurity flux measurements, for localizing impurity sources in ASDEX, the mirror system has been or may be used to measure:

- plasma ion temperatures from Doppler broadening of charge exchange recombination lines;
- toroidal and poloidal rotation from Doppler shifts of impurity lines (first test measurements have been made);
- local electron densities during pellet ablation from Stark broadening of D_α, D_β and D_γ lines during pellet-fueled discharges where the pellet could be observed direct [9];
- toroidal field strength from Zeeman splitting of C II or other lines in the edge region;
- deuterium/hydrogen density ratios;
- neutral beam components to determine beam species mixes;
- bremsstrahlung continuum in various visible regions to determine Z_{eff}-profiles.

References:

[1] A. Boileau, M. von Hellermann, L. D. Horton et. al., "Low-z impurity behaviour in JET from charge-exchange spectroscopy measurements", JET-P (89) 18.

[2] R. J. Goebner, P. Gohil, K. H. Burrell et. al., "Plasma rotation and electric field effects in H-mode in DIII-D", GA-A19562, (1989).

[3] K. Behringer, B. Denne, M. Forrest et. al., "Spectroscopic determination of impurity influx from localised surfaces", JET-P (89) 05.

[4] A. Pospieszczyk, P. Bogen, U. Samm, "Neutral particle fluxes emitted from the TEXTOR limiter", Proc. 11th Europ. Conf. on Controlled Fusion and Plasma Physics, Vol II, p. 417, Aachen (1983).

[5] J. Roth, G. Janeschitz, "Impurity production and transport in the divertor tokamak ASDEX", Nuclear Fusion 29, 6, p. 915-935 (1989).

[6] G. Fussmann, J. V. Hofmann, G. Janeschitz, H. R. Yang, "Sputtering flux measurements in the ASDEX divertor", IPP III/153 (1989).

[7] J. V. Hofmann, G. Fussmann, J.-M. Noterdaeme, F. Ryter, "Impurity flux measurements during ICRF heating in ASDEX", submitted to Fusion Engineering and Design.

[8] A. Boileau, M. von Hellermann, W. Mandl et. al., "Observations of motional Stark features in the Balmer spectrum of deuterium in the JET plasma", JET-P (89) 04.

[9] G. Wurden, J. Neuhauser, K. Büchl et. al., to be published.

Appendix

Transformation between polar coordinates (r,Θ,Φ) and step numbers (L,R,S)

As mentioned in section V, a selected point P inside the tokamak is usually given in toroidal coordinates (r, Θ, Φ); Fig. 5. To calculate the transformation of these coordinates into the step numbers (L, R, S), representing the position and orientation of the scanning mirror, we introduce, for convenience, a Cartesian coordinate system (x, y, z) with its origin on the axis and in the midplane of the torus. This system is connected to our polar coordinates by the well-known equations

$$x = (R_0 + r\cos\theta)\cos\phi$$
$$y = (R_0 + r\cos\theta)\sin\phi$$
$$z = r\sin\theta$$

To specify the origin of the scanning mirror system, which defines the longitudinal position L of the mirror, we shift this Cartesian system along the x-axis by the distance R_0+l_0 to produce the system (x′, y′, z′). The origin O′ is then the longitudinal position of the mirror when its step number is L = 0. This translation is then given by

$$x' = x - R_0 + l_0$$
$$y' = y$$
$$z' = z$$

For a step number L > 0 (usually 165,000 during the experiment) the mirror is at a distance L_m from O′. The step numbers R (rotation of the mirror around the axis (O′- m1) and S (movement of the mirror′s surface vector within the plane (O′- m1 - P) are expressed by the corresponding angles α and β, respectively, which describe the actual movement of the mirror. The distance of the point P from the mirror is denoted by ρ. Expressing (ρ, α, β) in terms of (x′, y′, z′) yields

$$\rho = \sqrt{(x' - L_m)^2 + (y'^2 + z'^2)}$$

$$\alpha = \text{arctg}(z'/y')$$

$$\beta = \text{arctg}\left(\frac{\sqrt{y'^2 + z'^2}}{x' - L_m}\right)$$

Finally, the step numbers R and S can be expressed in terms of α and β, while L may be chosen independently (instead ρ specifies the distance from the mirror):

$$L = L_0$$
$$R = R_0 + \alpha N_R$$
$$S = S_0 + \beta N_S$$

where

$$L_0 = L_m N_L, \quad N_L = 200200 \text{ steps / m}$$
$$R_0 = 5119, \quad N_R = 5000 \text{ steps / } \pi$$
$$S_0 = 6275, \quad N_S = 1000 \text{ steps / } \pi$$

With $R = R_0$ and $S = S_0$ the mirror's surface is perpendicular to the torus midplane, with its longer side parallel to the spectrometer's line of sight (O' - m1). N_R and N_S are the conversion factors from step numbers into radians and N_L the conversion from steps into meters.
As a result, we have the following sequence of transformations:

$$P\ (r, \theta, \phi) \Leftrightarrow P\ (x, y, z) \Leftrightarrow P\ (x', y', z') \Leftrightarrow P(\rho, \alpha, \beta) \Leftrightarrow P(\rho, R, S)_L$$

These transformations and additional information about the position of the selected point P (e.g. "above midplane", "towards north", "inner wall", "not accessible", ...) are supplied by a Fortran program running interactively during the experiment. A menu displaying 32 preselected points of frequent interest faciliates quick operation in the experiment; see Tab. 2. In addition, the step numbers and information may be looked up or printed out in the form of a menu or coordinate tables; see Tabs. 3, 4.

Figure captions:

Fig.1. Electronic block diagram of the ASDEX visible scanning mirror and detection system.

Fig. 2. Mechanical arrangement of the mirror system, showing the three directions of motion L, R and S of the mirror.

Fig. 3a. Sketch of the ASDEX midplane visualizing the position of the scanning mirror system relative to some other locations of interest. The grey-shaded area indicates the plasma.

Fig. 3b. Sketch of a poloidal ASDEX cross-section visualizing the accessible region during a poloidal scan of the mirror.

Fig. 4a. Schematic of the optical system indicating the main components: mirror, lenses L_1 and L_2, grating spectrometer and Reticon diode-array camera.

Fig. 4b. Some details of the actual optical setup to access, for example the gas valve and the SE neutral-beam injector.

Fig. 5. Video hardcopies from parts of the ASDEX divertor entrance during ohmic operation:

a. Inner edge of the lower divertor (poloidal view downward; see Fig. 3 b).

b. Water-cooled shielding plates at the outer entrance region of the lower divertor toroidally towards south at the position of the ICRH-SE antenna (see Figs. 3 a, b).

c. The throat region of the lower divertor, again towards south. The bent structure in the upper right quarter of the picture is the shielding between the outer and inner lower divertor slit (see Fig. 3 b).

Fig. 6. Vector diagram of the geometry used for the coordinate transformation.

Fig. 7a. A three-dimensional plot at the standard spectral range (around λ = 4300 Å) for plasma shot #28350 with additional heating by neutral injection (1.1 to 1.8 s) and lower hybrid (2.1 to 2.5 s).

Fig. 7b. The time dependence of the Cr-I, C-II, O-II and D_γ line intensities during the shot shown in Fig. 7 a, after integration of the specified lines.

Fig. 8. A 3D plot around λ = 3250 Å viewing the ICRH antenna. The dramatic rise of the Ti and Cu fluxes with the onset of ICRH heating is clearly revealed.

Fig. 9a. A 3D plot around λ = 6540 Å in the case of 3 poloidal scans during the discharge with additional heating by NI and LH.

Fig. 9b. Time evolution of the Cu-I, O-III, D_α and C-II line intensities during the plasma shot shown in Fig. 9 a. Note the very narrow peaks in the case of Cu-I in relation to D_α.

Fig. 10a. 3D plot in the case of modulated H_2S-gas puffing, starting at 0.5 s. The mirror is positioned in the direction of the gas valve; see Fig. 3 a. All five lines in this spectral range around λ = 5452 Å belong to the same S-II multiplet.

Fig. 10b. Time dependence of the S-II, λ = 5453.8 Å line intensity for the discharge shown in Fig. 10 a.

Tables:

Tab. 1. A list of spectral lines in the visible range identified in ASDEX discharges.

Tab. 2. Coordinates Θ, Φ and R, S for 32 of the most frequently used reference points in ASDEX (L = 165,000, corresponding to L_t = 226.8 cm; see Fig. 6.).

Tab. 3. Example of output produced by the coordinate transformation program for input = 8; (position Nº 8, given in Table 2.)

Tab. 4. Step numbers R and S for selected angles Θ and Φ (at L = 166,166, corresponding to L_t = 226 cm).

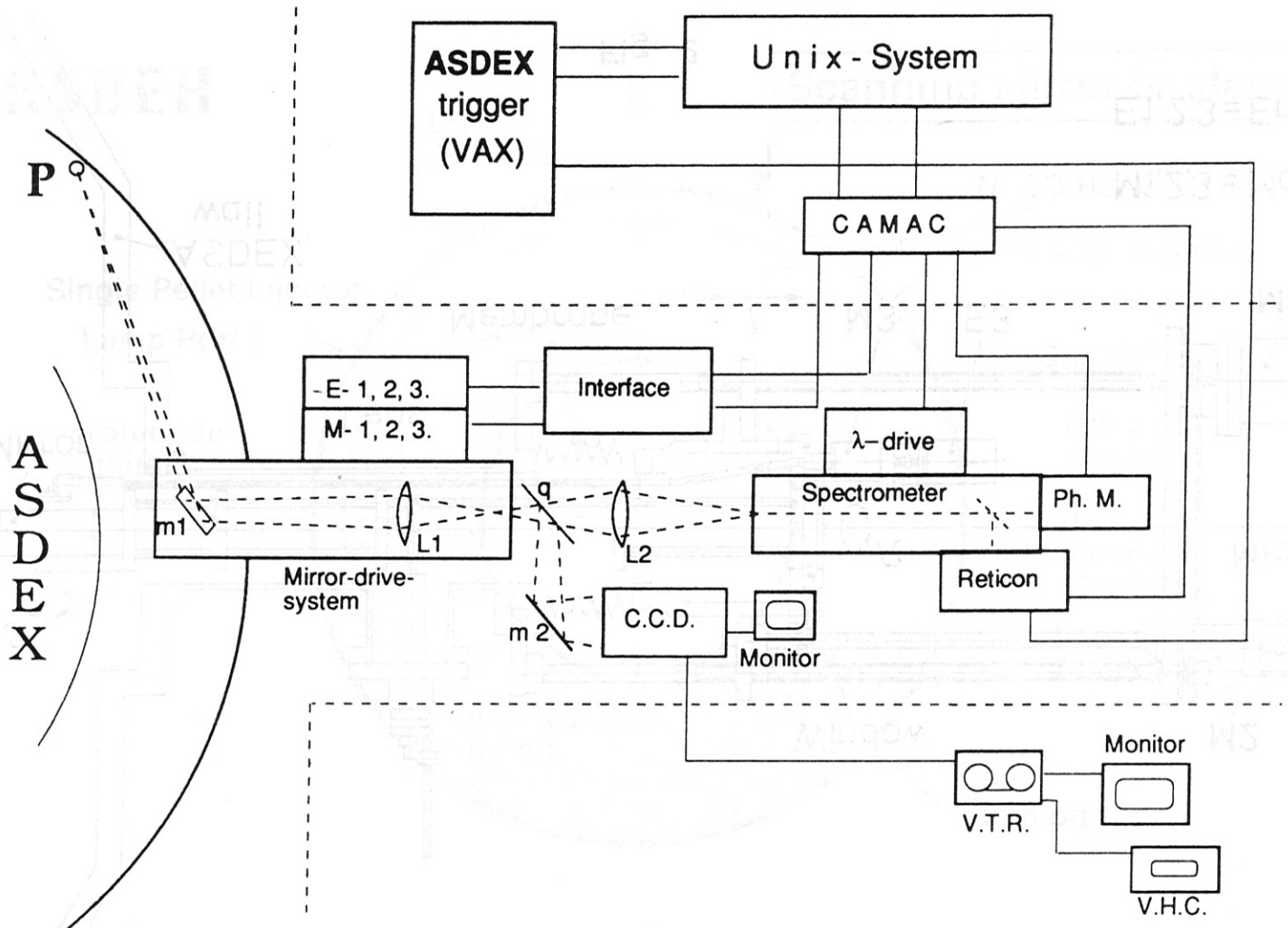
ASDEX
trigger
(VAX)
Unix - System
CAMAC
P
A
S
D
E
X
- E- 1, 2, 3.
M- 1, 2, 3.
Interface
λ– drive
Spectrometer
Ph. M.
Reticon
m1
L1
q
L2
Mirror-drive-
system
m 2
C.C.D.
Monitor
Monitor
V.T.R.
V.H.C.

Fig. 1

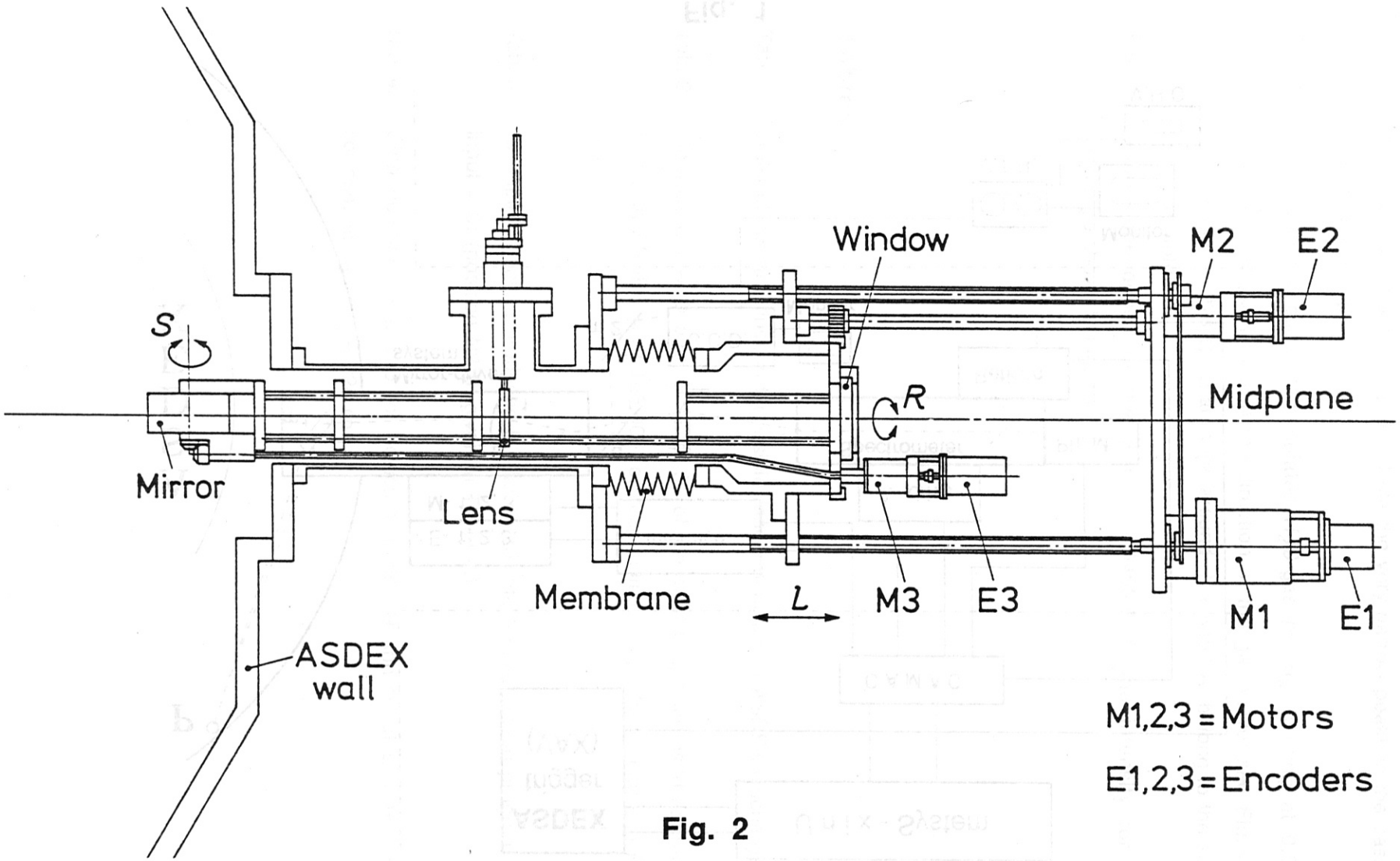
S
Window
M2
E2
R
Midplane
Mirror
Lens
Membrane
L
M3
E3
M1
E1
ASDEX
wall
M1,2,3 = Motors
E1,2,3 = Encoders

Fig. 2

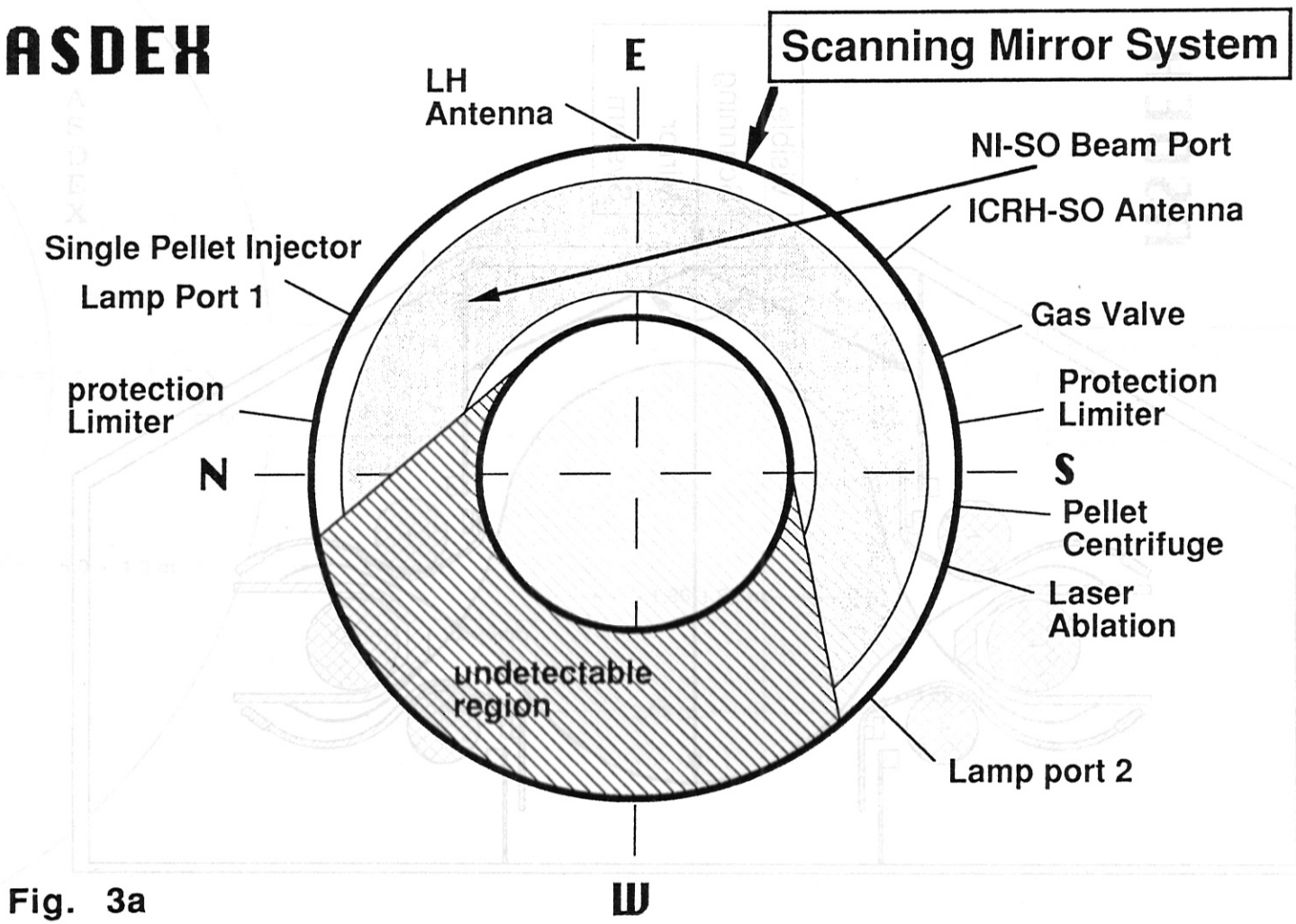
ASDEX
Scanning Mirror System
E
LH
Antenna
NI-SO Beam Port
ICRH-SO Antenna
Single Pellet Injector
Lamp Port 1
Gas Valve
protection
Limiter
Protection
Limiter
N
S
Pellet
Centrifuge
Laser
Ablation
undetectable
region
Lamp port 2
W

Fig. 3a

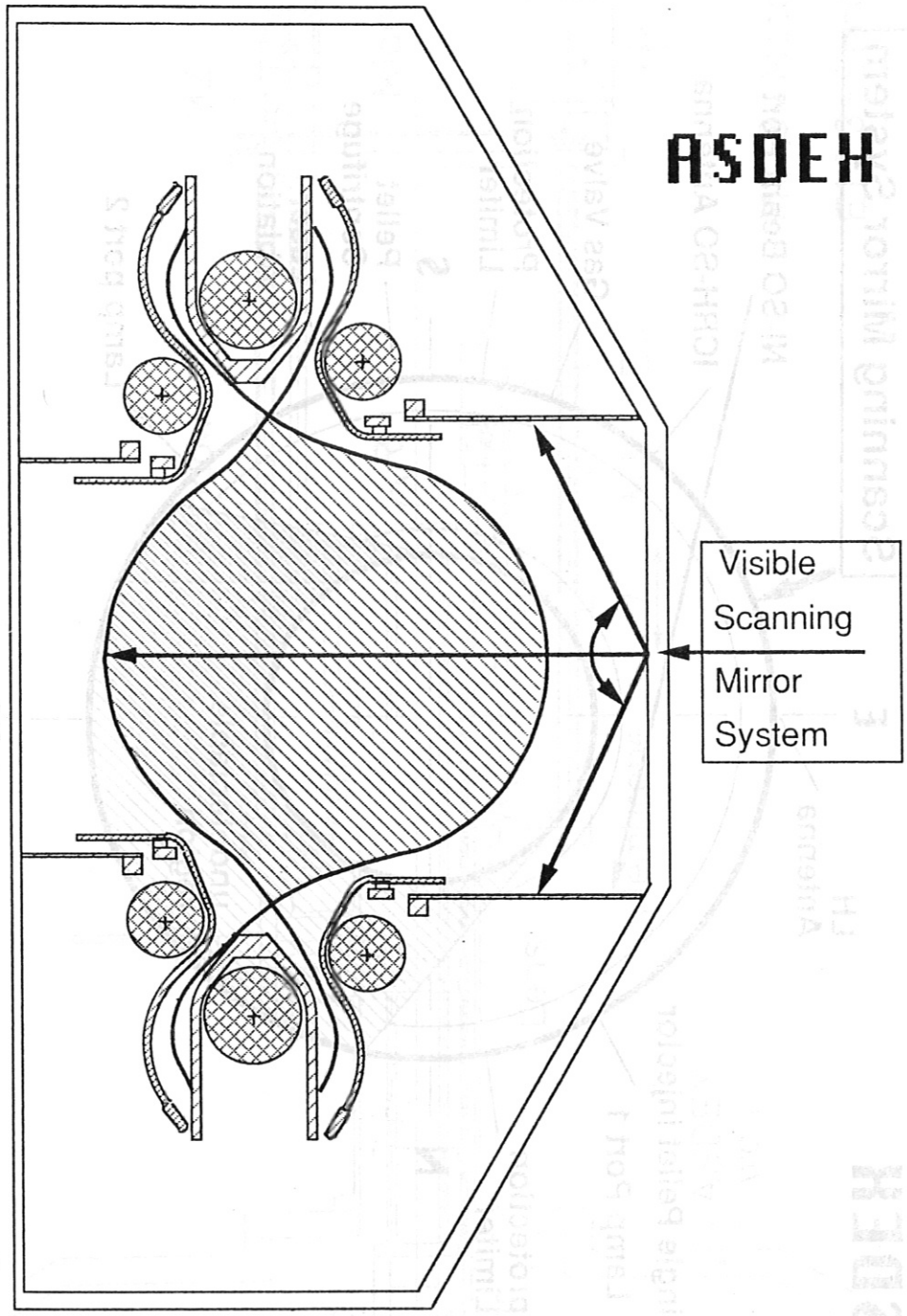

Fig. 3b

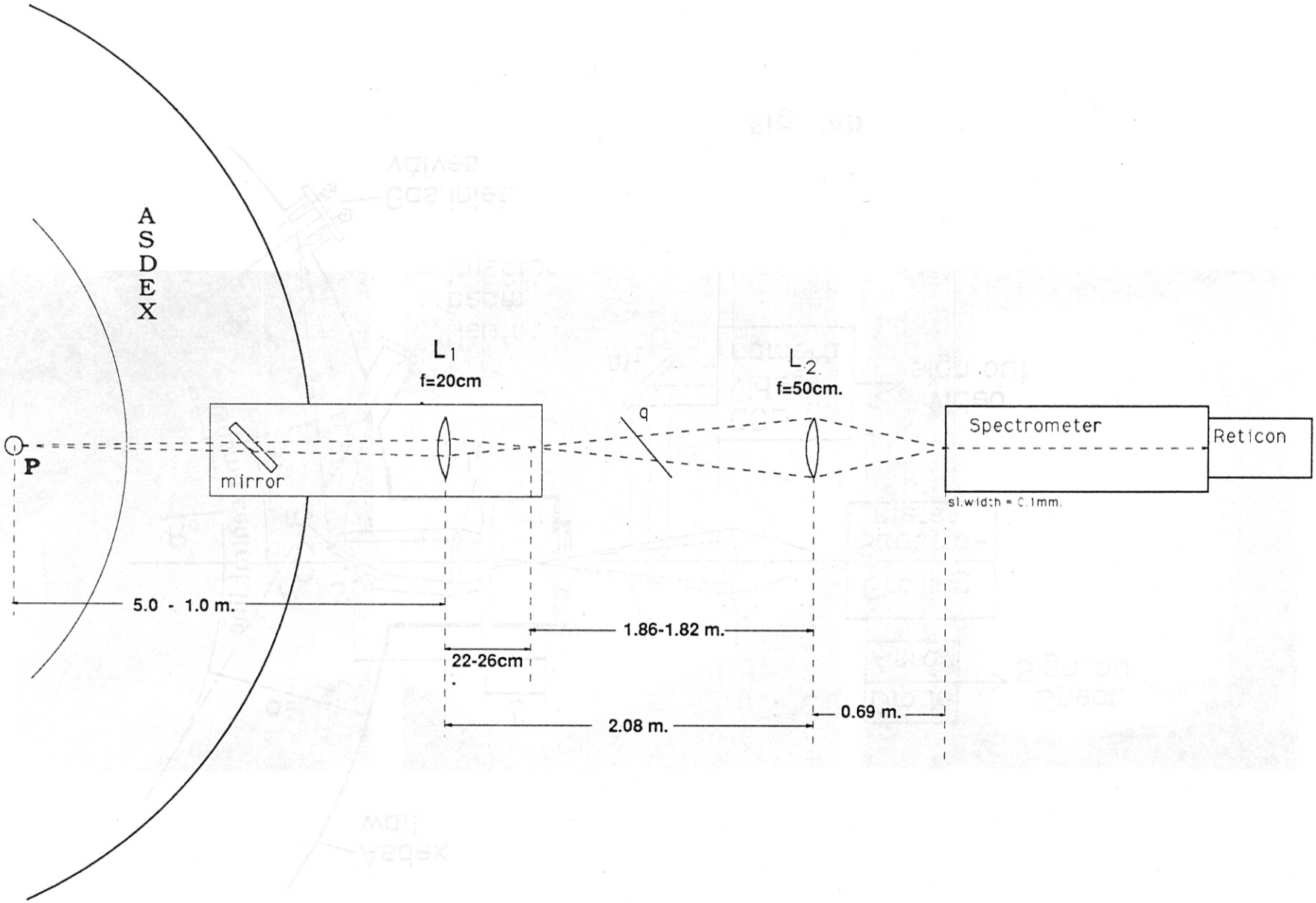
ASDEX
P
mirror
L1
f=20cm
q
L2
f=50cm.
Spectrometer
Reticon
sl.width = 0.1mm.
5.0 - 1.0 m.
22-26cm
1.86-1.82 m.
2.08 m.
0.69 m.

Fig. 4a

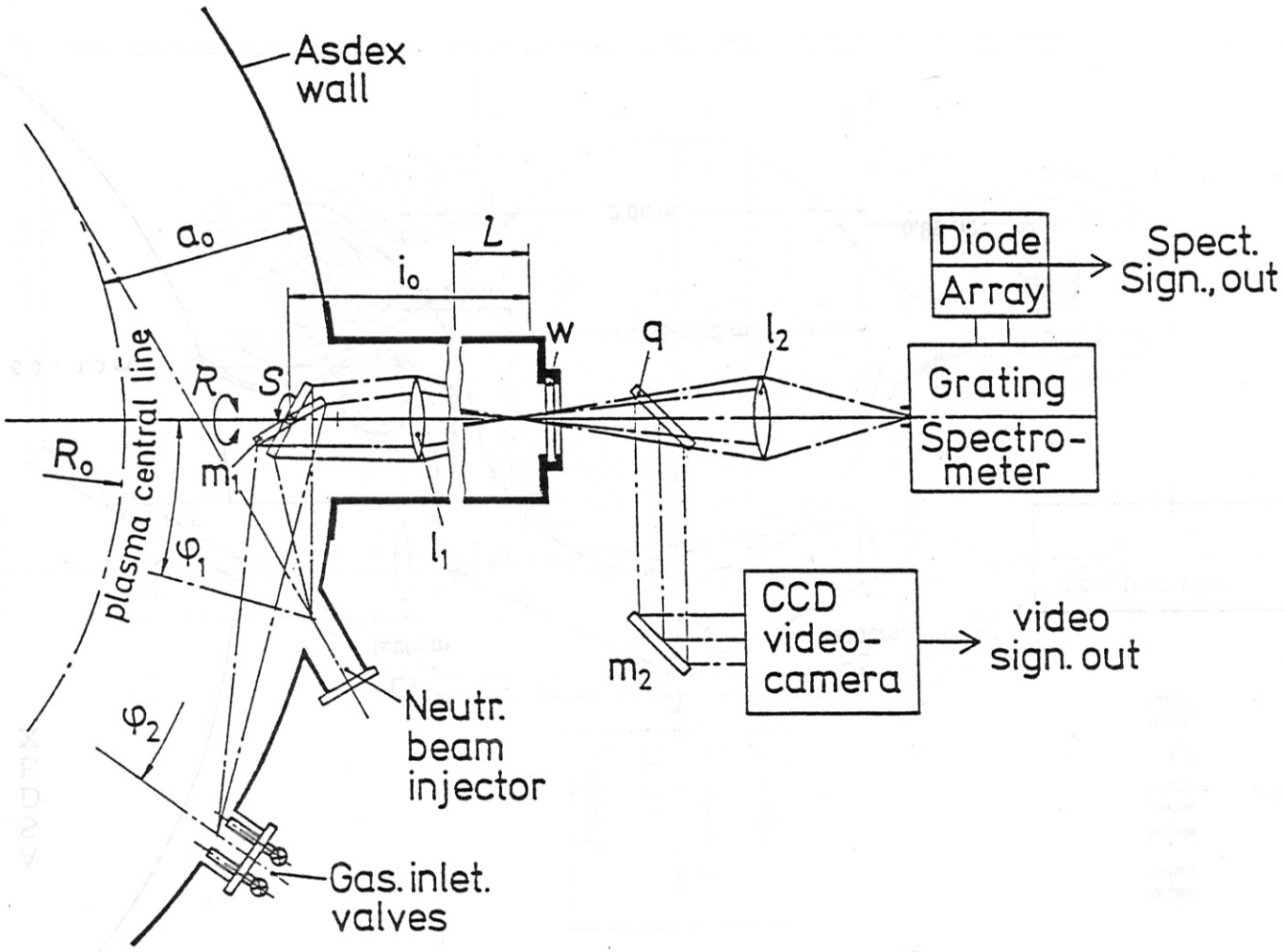
Asdex
wall
a_o
i_o
L
w
q
l_2
Diode
Array
Spect.
Sign., out
Grating
Spectro-
meter
R
S
R_o
m_1
plasma central line
φ_1
l_1
CCD
video-
camera
video
sign. out
m_2
φ_2
Neutr.
beam
injector
Gas. inlet.
valves

Fig. 4b

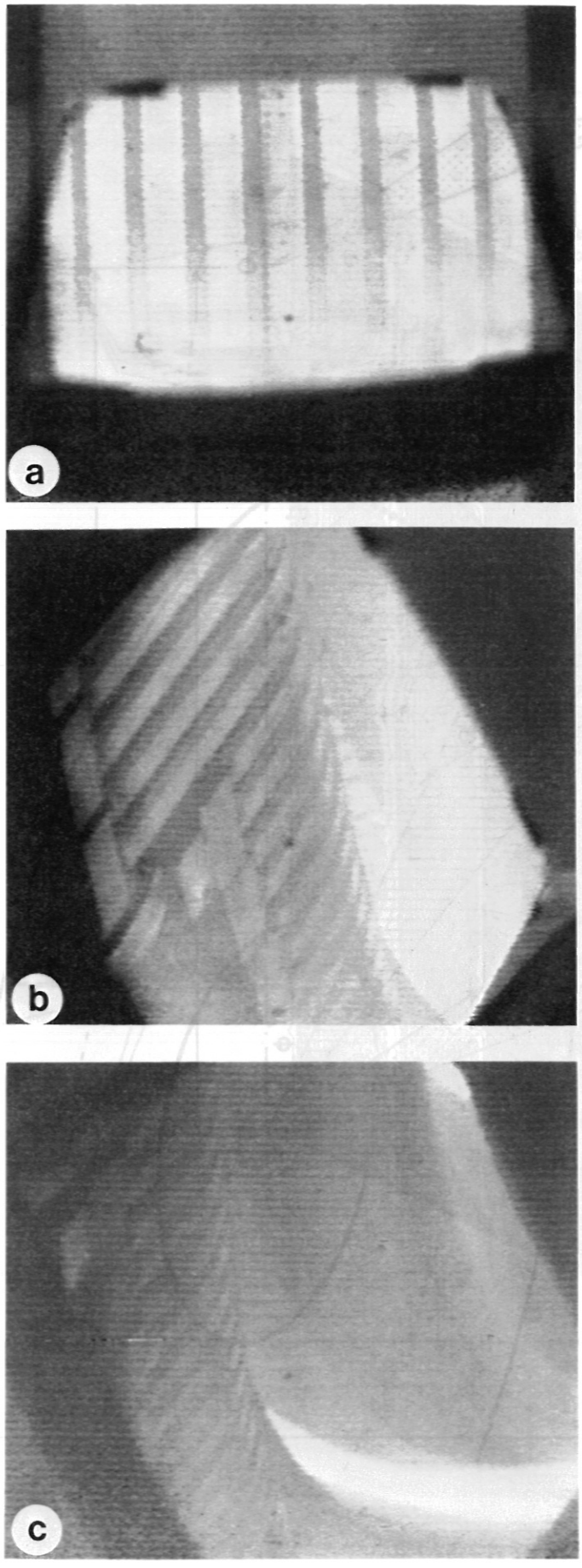

Fig. 5

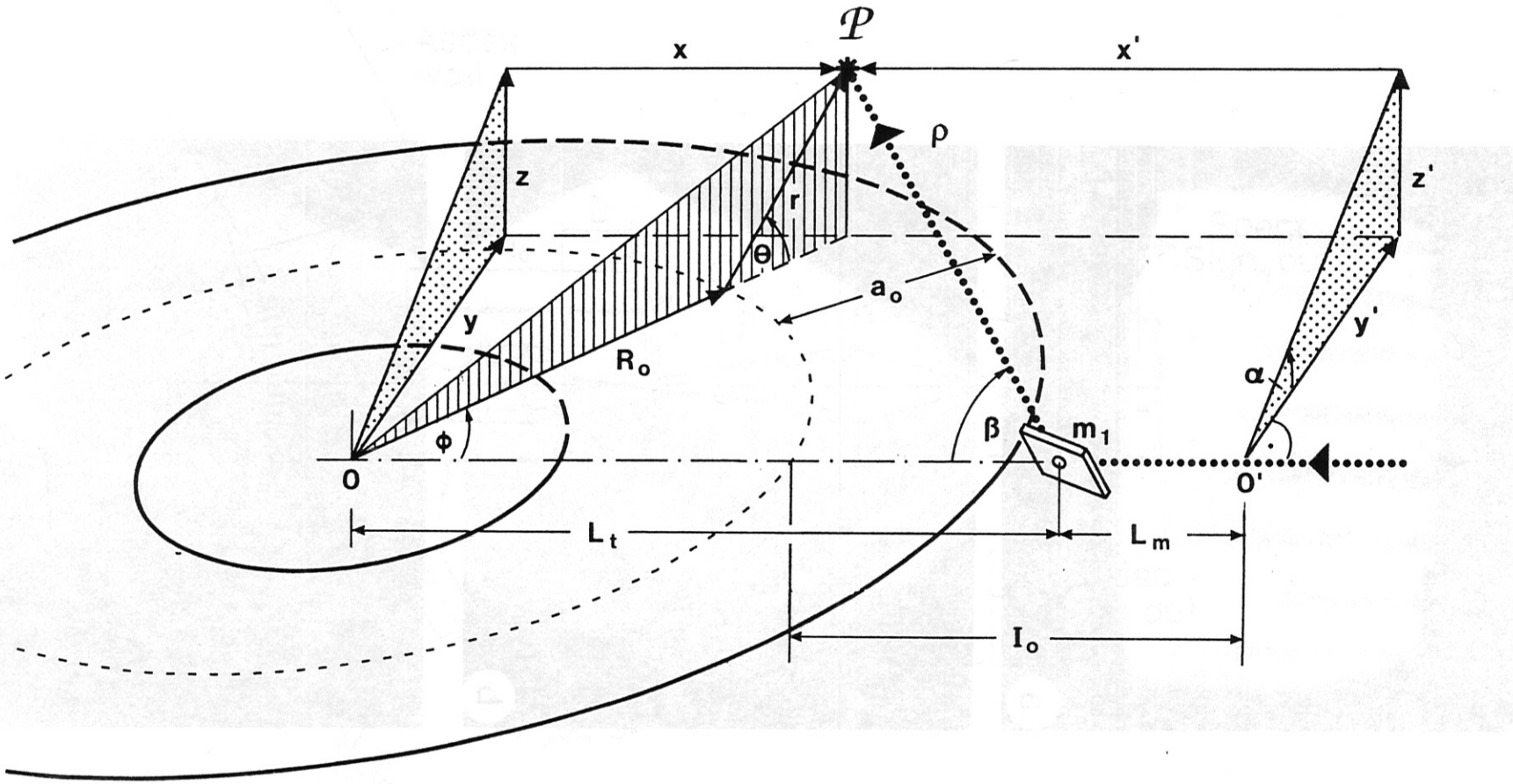

Fig. 6

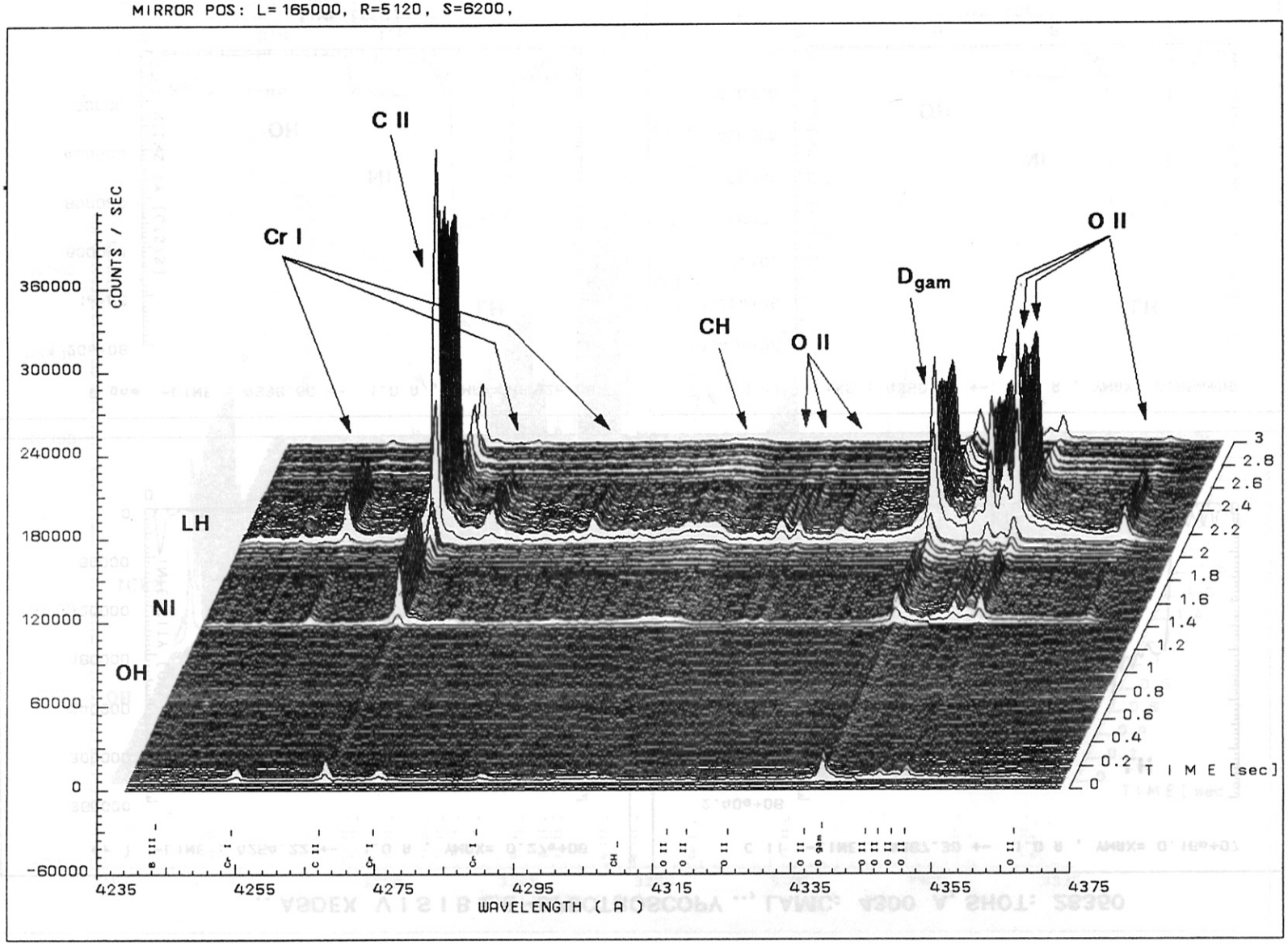
.. ASDEX V I S I B L E -SPECTROSCOPY .., LAMC: 4300 A, GR: 1200, SHOT: 28350
MIRROR POS: L= 165000, R=5120, S=6200,
C II
Cr I
CH
O II
D gam
O II
LH
NI
OH
COUNTS / SEC
360000
300000
240000
180000
120000
60000
0
-60000
4235
4255
4275
4295
4315
4335
4355
4375
WAVELENGTH (A)
3
2.8
2.6
2.4
2.2
2
1.8
1.6
1.4
1.2
1
0.8
0.6
0.4
0.2
0
T I M E [sec]

Fig. 7a

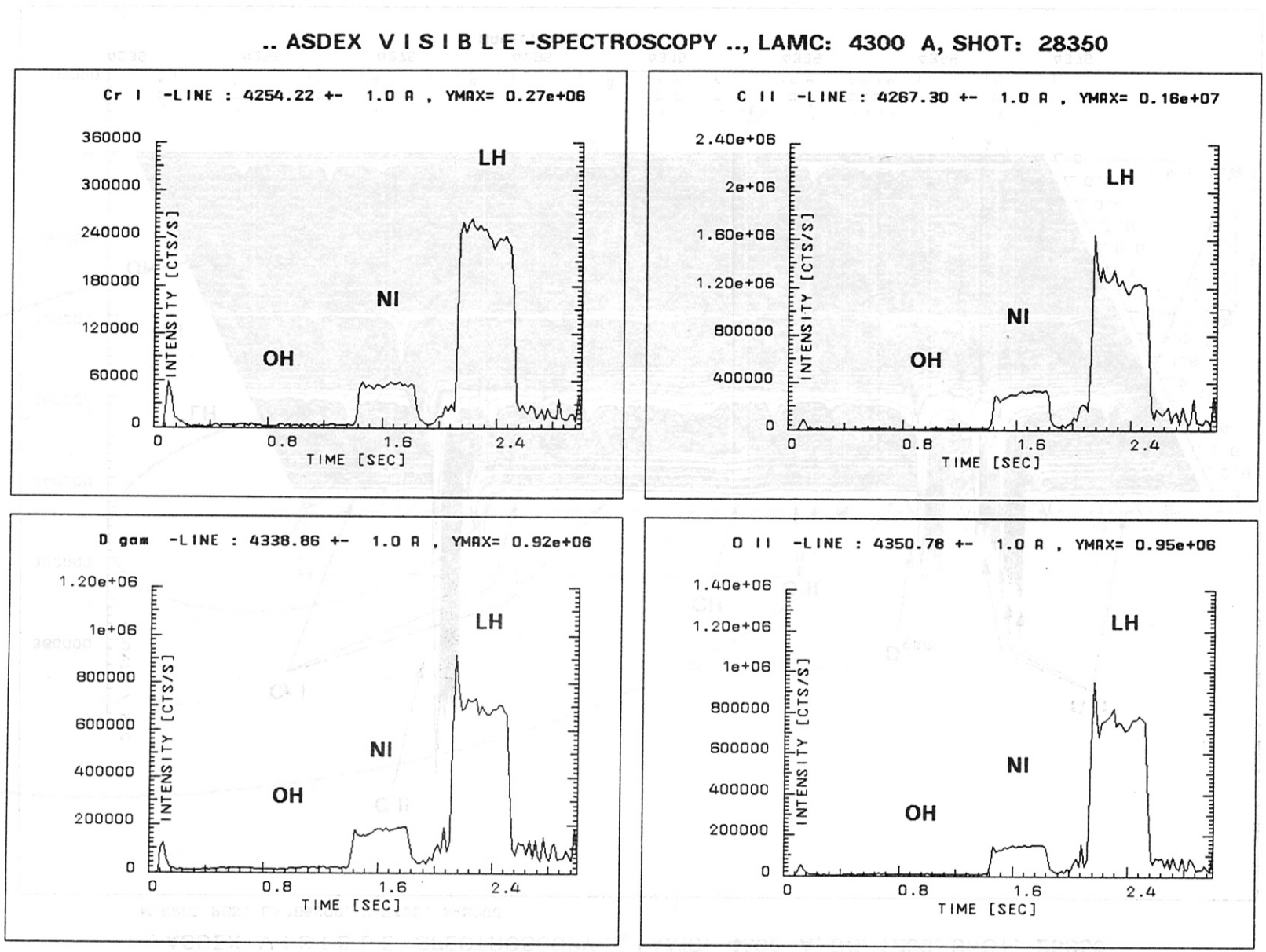
.. ASDEX V I S I B L E -SPECTROSCOPY .., LAMC: 4300 A, SHOT: 28350
Cr I -LINE : 4254.22 +- 1.0 A , YMAX= 0.27e+06
C II -LINE : 4267.30 +- 1.0 A , YMAX= 0.16e+07
D gam -LINE : 4338.86 +- 1.0 A , YMAX= 0.92e+06
O II -LINE : 4350.78 +- 1.0 A , YMAX= 0.95e+06
INTENSITY [CTS/S]
TIME [SEC]
LH
NI
OH

Fig. 7b

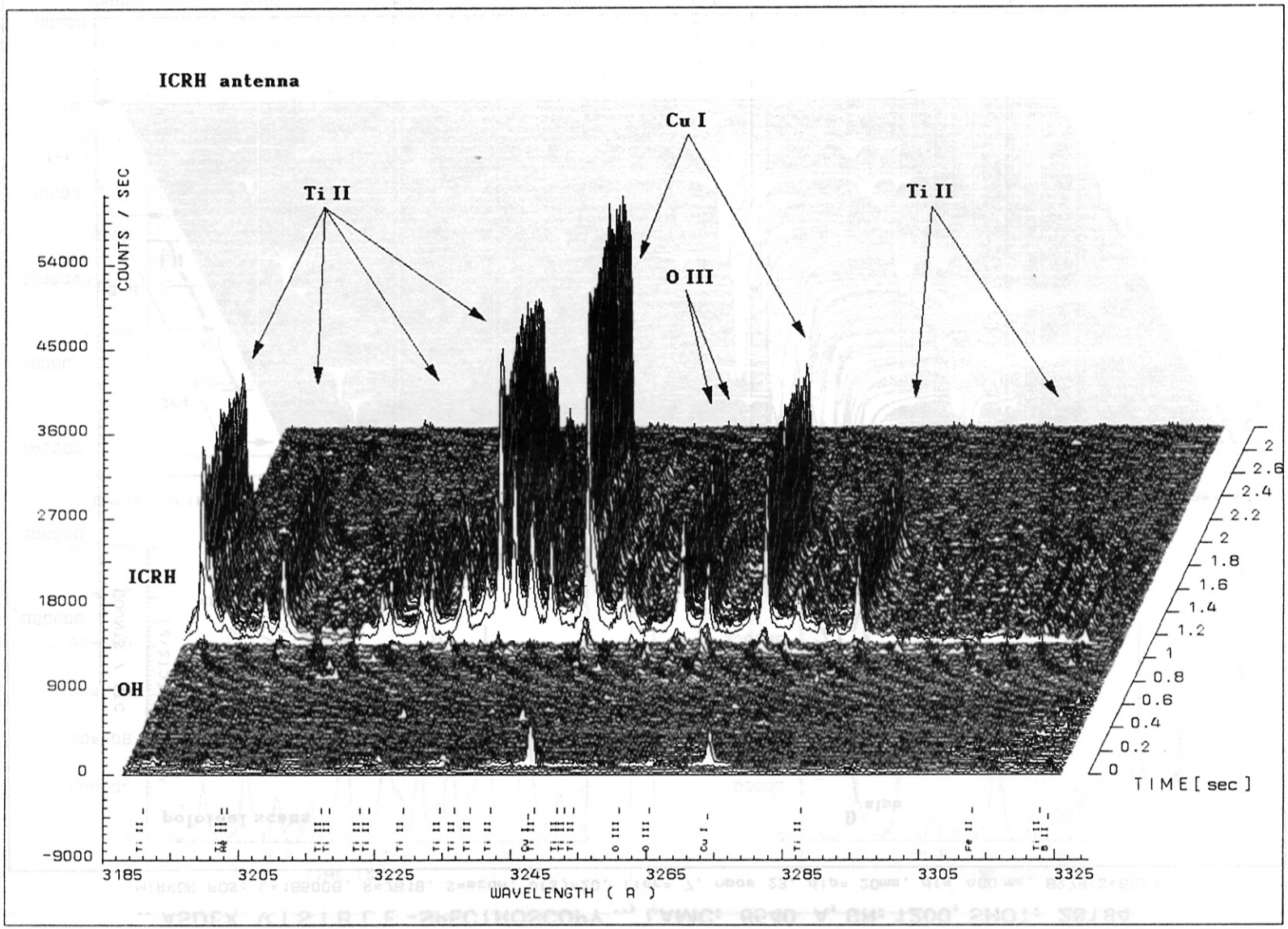
.. ASDEX V I S I B L E -SPECTROSCOPY .., LAMC: 3250 A, GR: 1200, SHOT: 28287
MIRROR POS: L= 165000, R=5120, S=6199,
ICRH antenna
Cu I
Ti II
Ti II
O III
ICRH
OH
COUNTS / SEC
54000
45000
36000
27000
18000
9000
0
-9000
3185
3205
3225
3245
3265
3285
3305
3325
WAVELENGTH (A)
2
2.6
2.4
2.2
2
1.8
1.6
1.4
1.2
1
0.8
0.6
0.4
0.2
0
TIME[sec]

Fig. 8

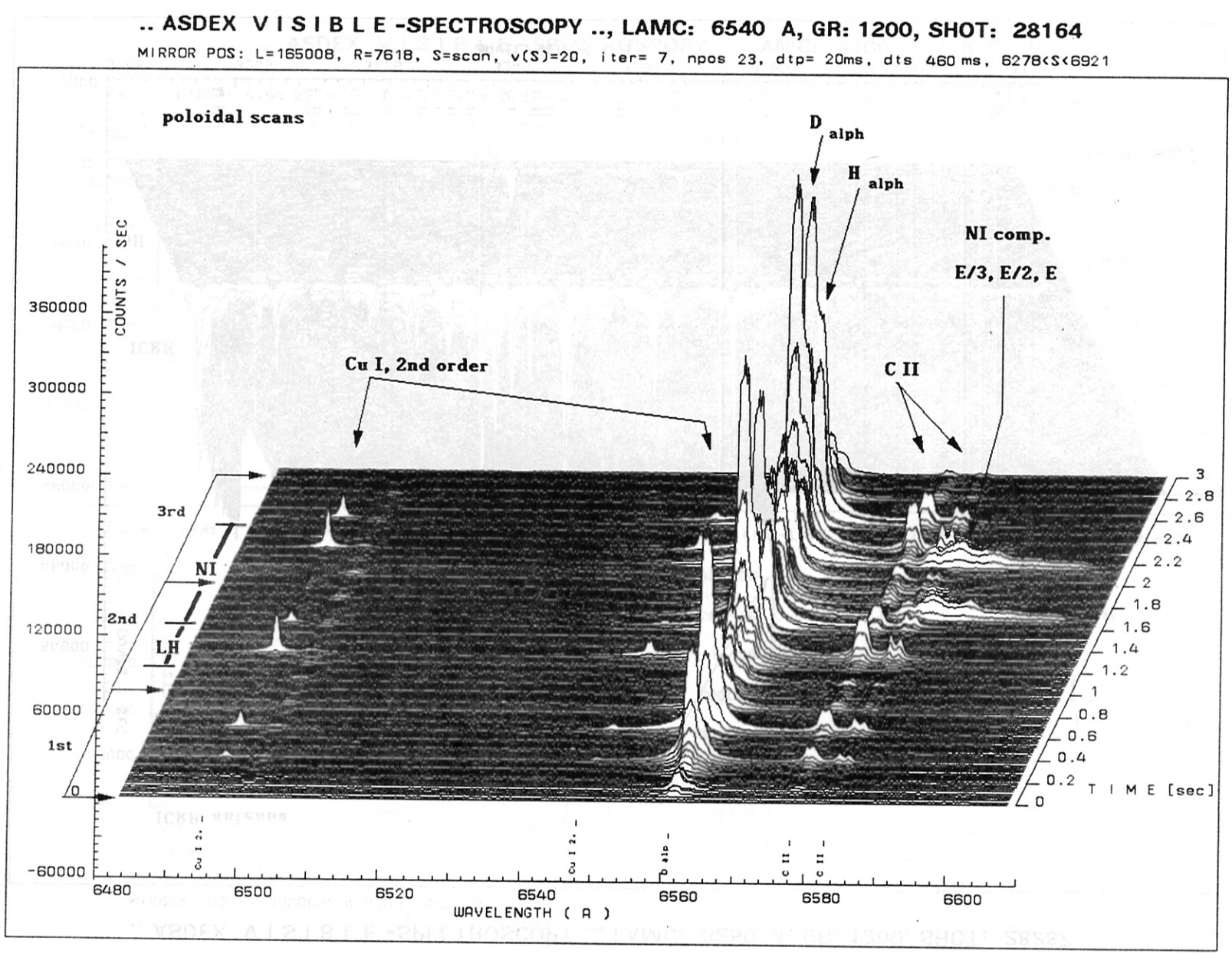
.. ASDEX V I S I B L E -SPECTROSCOPY .., LAMC: 6540 A, GR: 1200, SHOT: 28164
MIRROR POS: L=165008, R=7618, S=scan, v(S)=20, iter= 7, npos 23, dtp= 20ms, dts 460 ms, 6278<S<6921
poloidal scans
D alph
H alph
NI comp.
E/3, E/2, E
Cu I, 2nd order
C II
3rd
NI
2nd
LH
1st
COUNTS / SEC
360000
300000
240000
180000
120000
60000
0
-60000
6480
6500
6520
6540
6560
6580
6600
WAVELENGTH (A)
3
2.8
2.6
2.4
2.2
2
1.8
1.6
1.4
1.2
1
0.8
0.6
0.4
0.2
0
T I M E [sec]

Fig. 9a

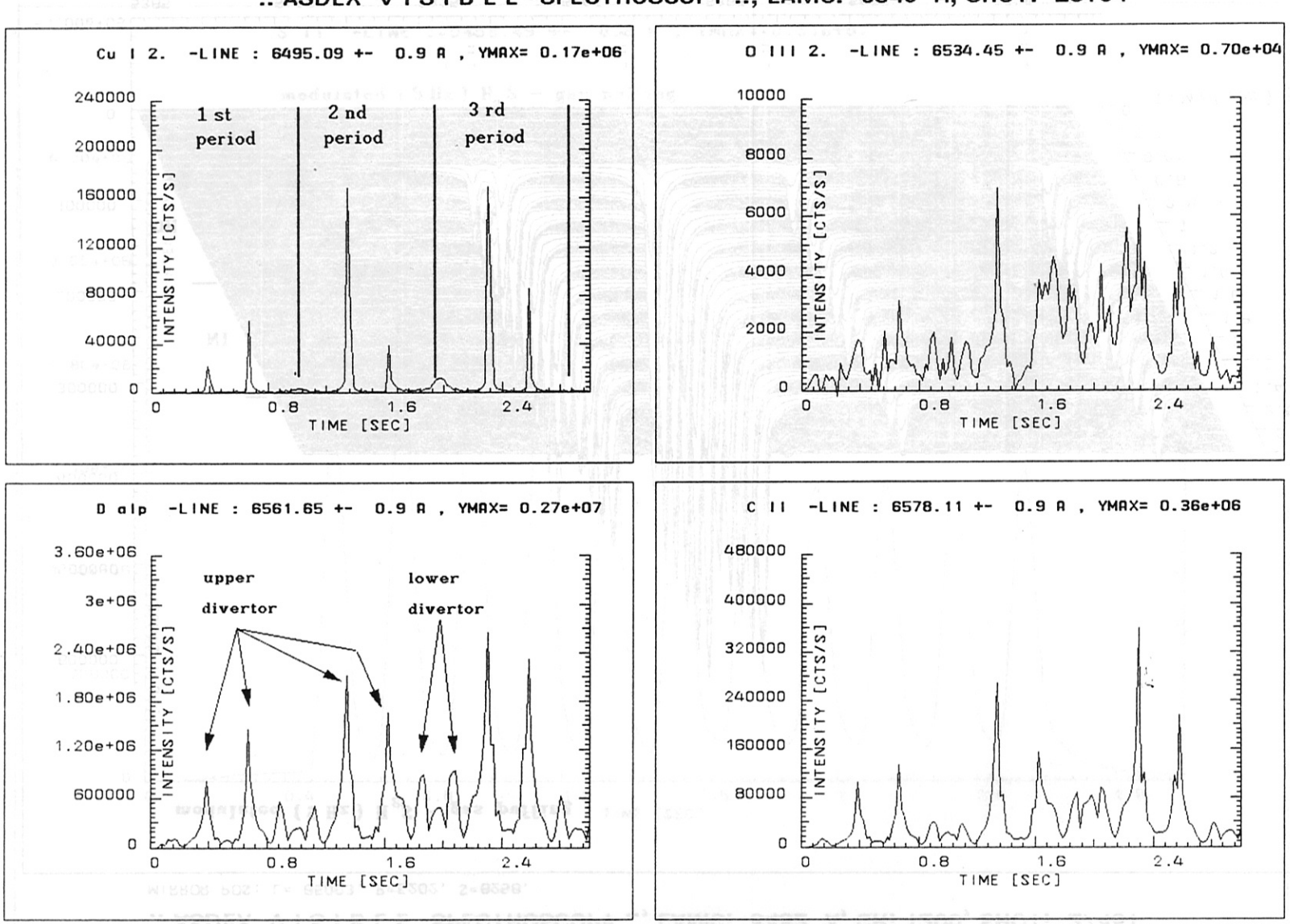
.. ASDEX V I S I B L E -SPECTROSCOPY .., LAMC: 6540 A, SHOT: 28164
Cu I 2. -LINE : 6495.09 +- 0.9 A , YMAX= 0.17e+06
1 st period
2 nd period
3 rd period
INTENSITY [CTS/S]
TIME [SEC]
O III 2. -LINE : 6534.45 +- 0.9 A , YMAX= 0.70e+04
D alp -LINE : 6561.65 +- 0.9 A , YMAX= 0.27e+07
upper divertor
lower divertor
C II -LINE : 6578.11 +- 0.9 A , YMAX= 0.36e+06

Fig. 9b

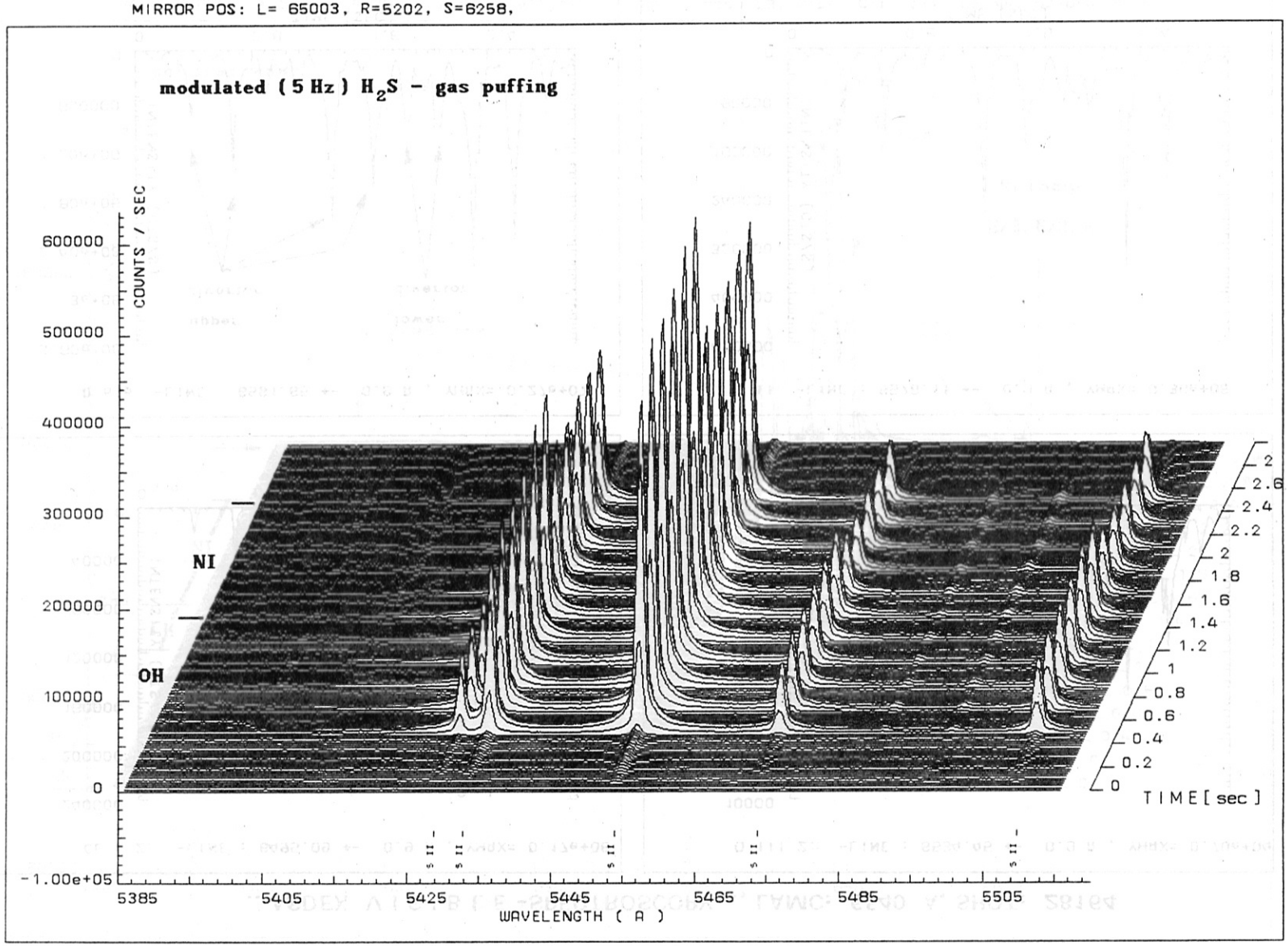
.. ASDEX V I S I B L E -SPECTROSCOPY .., LAMC: 5452 A, GR: 1200, SHOT: 27451
MIRROR POS: L= 65003, R=5202, S=6258,
modulated (5 Hz) H2S - gas puffing
COUNTS / SEC
600000
500000
400000
300000
200000
100000
0
-1.00e+05
NI
OH
5385
5405
5425
5445
5465
5485
5505
WAVELENGTH (A)
TIME[sec]
2
2.6
2.4
2.2
2
1.8
1.6
1.4
1.2
1
0.8
0.6
0.4
0.2
0

Fig. 10a

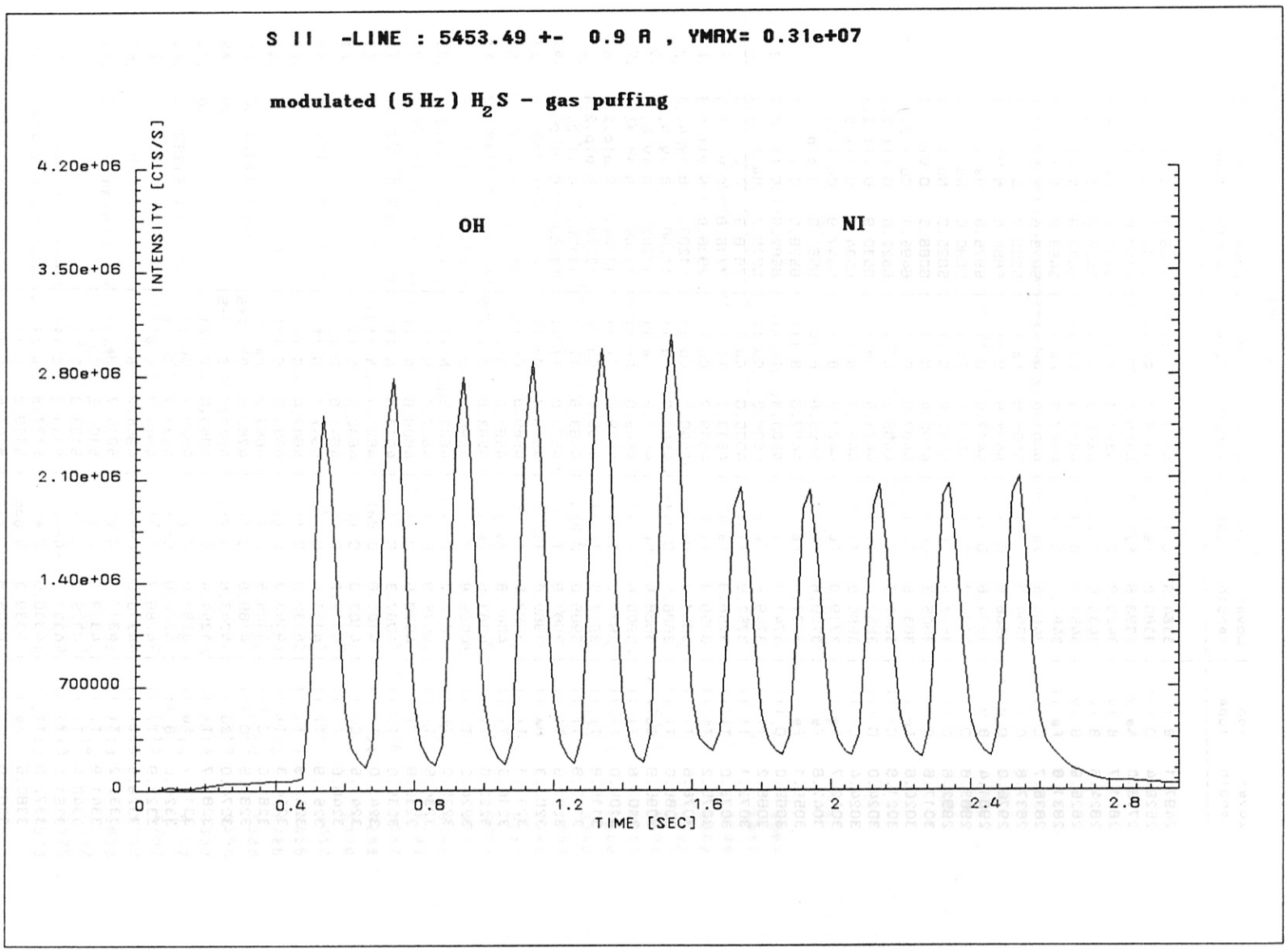
.. ASDEX V I S I B L E -SPECTROSCOPY .., LAMC: 5452 A, SHOT: 27451
S II -LINE : 5453.49 +- 0.9 A , YMAX= 0.31e+07
modulated (5 Hz) H_2S - gas puffing
INTENSITY [CTS/S]
4.20e+06
3.50e+06
2.80e+06
2.10e+06
1.40e+06
700000
0
OH
NI
0
0.4
0.8
1.2
1.6
2
2.4
2.8
TIME [SEC]

Fig. 10b

wave-length	ion type	wave-length	ion type	wave-length	ion type	wave-length	ion type
2497.1	B I	3384.9	O III	4347.4	O II	5145.2	C II
2529.4	O III	3389.8	Fe I	4348.1	Ar II	5151.1	C II
2778.0	Ne X	3396.6	Fe I	4349.4	O II	5290.6	C VI
2821.7	B IV	3409.8	O II	4351.3	O II	5411.5	He II
2824.6	B IV	3433.8	C VI	4366.9	O II	5428.6	S II
2825.9	B IV	3451.4	B II	4371.3	Ar II	5432.8	S II
2831.6	Fe II	3480.1	O III	4387.9	He I	5453.8	S II
2836.7	C II	3484.5	Fe I	4401.0	Ar II	5473.6	S II
2837.6	C II	3504.9	Ti II	4404.8	Fe I	5509.7	S II
2976.0	O VIII	3568.5	O II	4414.9	O II	5669.4	N VII
2981.4	B V	3574.6	O II	4417.0	O II	5875.6	He I
2983.8	O III	3578.7	Cr I	4443.8	Ti II	5890.0	Na I
2992.6	C II	3593.5	Cr I	4452.4	O II	5895.9	Na I
3017.6	Cr II	3605.3	Cr I	4465.4	O II	6068.3	O VIII
3020.6	Fe I	3635.5	Ti I	4467.9	O II	6495.1	Cu I 2.
3021.6	Cr II	3642.7	Ti I	4469.3	O II	6522.0	O III 2.
3024.0	O III	3653.5	Ti I	4471.5	He I	6530.9	O III 2.
3024.4	Cr II	3685.2	Ti II	4472.1	B II	6534.6	O III 2.
3042.7	Fe I	3719.9	Fe I	4487.5	B III	6547.9	Cu I 2.
3047.6	Fe I	3729.8	Ti I	4490.8	B IV	6561.0	D alp
3059.1	Fe I	3737.1	Fe I	4497.6	B III	6578.0	C II
3065.0	O III	3741.1	Ti I	4501.3	Ti II	6582.9	C II
3066.2	Ti II	3749.5	Fe I	4506.0	Cu II	6678.2	He I
3072.1	Ti II	3752.9	Ti I	4530.8	Cu I	7618.5	C V
3073.0	Ti II	3758.9	Fe I	4533.2	Ti I	7716.8	C VI
3075.2	Ti II	3759.3	Ti I	4539.7	Cu I	7926.0	N VII
3078.6	Ti II	3883.7	Ne X	4540.2	Cu II	11287.	B IV 4.
3088.0	Ti II	3886.9	O VIII	4541.0	Cu II	11298.	B IV 4.
3095.9	Cu XIX	3888.6	He I	4541.6	He II	11303.	B IV 4.
3103.8	Ti II	3900.6	Ti II	4545.0	Ar II	11345.	B ?? ?.
3105.0	Ti II	3911.2	Ti I	4549.6	Ti II	13122.	D alp.2.
3119.8	Ti II	3913.5	Ti II	4555.7	Cu II	13126.	H alp.2.
3190.9	Ti II	3969.0	D eps	4563.8	Ti II	13156.	C II 2.
3202.5	Ti II	3981.8	Ti I	4572.0	Ti II	13166.	C II 2.
3203.3	He II	3989.8	Ti I	4579.3	Ar II		
3217.1	Ti II	3998.6	Ti I	4589.9	Ar II		
3218.3	Ti II	4045.8	Fe I	4591.0	O II		
3222.8	Ti II	4063.6	Fe I	4593.8	C III 2		
3224.2	Ti II	4069.8	O II	4596.2	O II		
3229.2	Ti II	4072.2	O II	4601.5	N II		
3234.5	Ti II	4075.9	O II	4607.1	N II		
3236.6	Ti II	4078.9	O II	4609.6	Ar II		
3239.0	Ti II	4097.3	O II	4613.9	N II		
3242.0	Ti II	4100.6	D del	4621.4	N II		
3247.5	Cu I	4103.0	O II	4630.5	N II		
3248.6	Ti II	4119.2	O II	4641.8	O II		
3251.9	Ti II	4121.5	O II	4643.1	N II		
3252.9	Ti II	4132.8	O II	4647.4	C III		
3254.3	Ti II	4153.3	O II	4651.0	C III		
3261.0	O III	4185.5	O II	4685.7	He II		
3265.5	O III	4189.8	O II	4789.5	Br II+5		
3274.0	Cu I	4243.6	B III	4821.7	Br II+5		
3287.7	Ti II	4254.4	Cr I	4860.0	D bet		
3312.7	Fe II	4267.0	C II	4909.7	Cu II		
3324.0	B II	4274.8	Cr I	4931.7	Cu II		
3322.9	Ti II	4289.7	Cr I	4944.7	C V		
3329.5	Ti II	4310.0	CH m	4944.7	B V		
3335.2	Ti II	4317.1	O II	5015.7	He I		
3341.9	Ti II	4319.9	O II	5105.5	Cu I		
3349.4	Ti II	4325.8	O II	5133.0	C II		
3361.2	Ti II	4331.2	Ar II	5133.3	C II		
3372.8	Ti II	4336.9	O II	5137.3	C II		
3380.5	Fe I	4339.3	D gam	5139.2	C II		
3383.8	Ti II	4345.6	O II	5143.5	C II		

Table 1

****
*
* M I R R O R P O S I T I O N S
*
****

Datum: 13 9 ,'89.

M E N U :

No.	Name:	PHI:	THETA:	R:	S:
1.	N.N.O. Pellet shot investigation.	92	0	5119	6803
2.	N.O. Lamp port. (Fast film.)	82	10.5	5200	6847
3.	N.O. Glimmentladung.	58	0	5119	6904
4.	O.N.O. HCN-Laser.	42	0	5119	6952
5.	O. HF-Heizung.	20	0	5119	6972
6.	O.S.O. Spiegel.	-11	-150	6414	6493
7.	S.O. Neutralt. Injector.	-18	0	5119	6111
8.	S.O. ICRH-Antenna.	-30	0	5119	6200
9.	S.S.O. FIR-Streuung-Spiegel.	-47.5	-54	5564	6260
10.	S.S.O. Gaseinlass Ventil.	-49.5	-12.5	5202	6258
11.	S. Schutzlimiter.	-61.5	0	5119	6269
12.	S. Trennspalt Abdeckung.	-70	0	5119	6285
13.	S. Pellet Zentrifuge.	-76	0	5119	6291
14.	S. Laser Ablation.	-87	0	5119	6321
15.	S.S.W. Randschicht-Streuung.	-101	0	5119	6365
16.	S.W. Lamp Position.	-114	0	5119	6389
17.	S. LOWER Divertor (middle)	-30	-105	6066	6337
18.	S. " " slit (outer)	-30	-82	5854	6299
19.	S. " " " (inner)	-30	-120	6083	6370
20.	N. UPPER Divertor (middle)	30	105	6066	6818
21.	N. " " slit (outer)	30	82	5854	6856
22.	N. " " " (inner)	30	120	6083	6785
23.	O. LOWER Divertor (middle)	0	-105	7619	6388
24.	O. " " slit (outer)	0	-95	7619	6358
25.	O. " " " (inner)	0	-110	7619	6397
26.	O. UPPER Divertor (middle)	0	105	7619	6767
27.	O. " " slit (outer)	0	95	7619	6797
28.	O. " " " (inner)	0	110	7619	6758
29.	U. Ringspannung (inner)	0	156	7619	6638
30.	U. " (outer)	0	34.5	7619	6922
31.	Central inner wall.	0	180	7619	6575
32.	Back reflection; looking out!	0	0	7619	7573

****

Table 2

```
                              *  *
=======================================================================
                        The   S T E P N U M B E R S
              of the coordinates of the point No.  8  of ASDEX:
                     Radial position: 48. cm
                         S.O.  ICRH-Antenna.
                      The distance from the mirror: 1.15 m
                 THETA=   0. deg.            PHI -30.0 deg.
-----------------------------------------------------------------------
                        This is an outer-wall position
                                    O. K.
                      We are in the SOUTHERN haemisphere.
                       R0=5119                 S0=6575
-----------------------------------------------------------------------
                                        |
      /in rad's:/ ALPHA=  0.            |   BETA= -1.194
                                        |
      /in degr's:/   " =     0          |     " =    -68
-----------------------------------------------------------------------
                                  C o o r d i n a t e s:
                                        |
                 Rotation:              |   Mirror angle:
                                        |
      Coordinates:    R =   5119 st     |     S =   6200 st
        /in steps/                      |
                                        |
                        Longitudinal mirror-position:
               L=165000 steps;              61.6 cm.
-----------------------------------------------------------------------
                                    O.  K.
                                In the midplane...
=======================================================================
```

Table 3

R E S U L T S / In Table : /

If Theta, and Phi in the same time equal zero,
that point doesn't exist in the tokamak!
L =166166 /step/ I0 =0.61 /m/

R O T A T I O N S , (R):

Theta:	-180.	-135.	-90.	-45.	0.	45.	90.	135.
Phi:								
-90.	5119	5667	5688	5447	5119	9791	9550	9571
-75.	5119	5685	5706	5458	5119	9780	9532	9553
-60.	5119	5744	5767	5496	5119	9742	9471	9494
-45.	5119	5866	5892	5576	5119	9662	9346	9372
-30.	5119	6109	6140	5749	5119	9489	9098	9129
-15.	5119	6624	6654	6200	5119	9038	8584	8614
0.	7619	7619	7619	7619	7619	7619	7619	7619
15.	5119	8614	8584	9038	5119	6200	6654	6624
30.	5119	9129	9098	9489	5119	5749	6140	6109
45.	5119	9372	9346	9662	5119	5576	5892	5866
60.	5119	9494	9471	9742	5119	5496	5767	5744
75.	5119	9553	9532	9780	5119	5458	5706	5685

M I R R O R A N G L E S, (S):

-90.	6443	6415	6369	6339	6330	6816	6786	6740
-75.	6432	6398	6341	6301	6288	6854	6814	6757
-60.	6429	6388	6317	6265	6246	6890	6838	6767
-45.	6438	6388	6300	6230	6204	6925	6855	6767
-30.	6465	6404	6296	6202	6162	6953	6859	6751
-15.	6513	6434	6311	6188	6118	6967	6844	6721
0.	6575	6454	6328	6201	7573	6954	6827	6701
15.	6642	6434	6311	6188	7037	6967	6844	6721
30.	6690	6404	6296	6202	6993	6953	6859	6751
45.	6717	6388	6300	6230	6951	6925	6855	6767
60.	6726	6388	6317	6265	6909	6890	6838	6767
75.	6723	6398	6341	6301	6867	6854	6814	6757

Table 4